ISSN 1024-588X. Вісник Львівського університету. Серія фізична. 2012. Випуск 47. С. 248-277
Visnyk of the Lviv University. Series Physics. 2012. Issue 47. P. 248-277

УДК 524.37-36, 524.78+524.523
PACS 98.38.Ly, 98.58.Li, 98.38.Hv, 98.58.Hf, 98.52.Nr, 07.05Tp

REVIEW OF NEBULAR ASTROPHYSICS

B. Melekh

Ivan Franko National University of Lviv, Kyrylo and Mefodiy St., 8, 79005 Lviv, Ukraine

A brief review of the research history of the nebular objects is represented. The basic modern methods for determining the physical characteristics and chemical compositions in the different nebular enviroments are described. The new approaches to the investigation of planetary nebulae and HII regions, developed at the astrophysics department of Lviv National University, as well as the new physical results, obtained using these approaches, are considered.

Key words: planetary nebulae, HII regions, photoionization modelling, emission lines, nebular diagnostics.

1 Introduction

Planetary nebulae, giant H II regions, supernovae remnants, novae envelopes, nuclei of the active galaxies... The beauty of these objects allows us to call them "flowers of the Universe". They exist as transformers of the ionizing radiation into non-ionizing one. The physical conditions in these objects are completly different from the ones in stars and planets atmospheres.

In present paper the short overview of the investigation history as well as modern methods for the diagnostic and modelling of the nebular objects is done.

In Section 2, we will see how nebular objects were discovered, and will trace the becoming of the real understanding of their nature. Also, in this Section the general characteristics of the different kinds of the nebular objects are briefly overviewed.

Section 3 represents the general overview of the simple diagnostic methods.

The approaches to the chemical composition determination in these objects are considered in Section 4. Several methods that take into account the unobserved ionization stages are generally overviewed. It is noted the crucial role of the photoionization modelling in tasks on the chemical composition determination.

In Section 5, the basic equation of the photoionization modelling as well as different assumption which are usually used in this modelling are considered. The aim of this Section is to introduce the reader with the main equations that describe physical conditions in nebular objects as well as show different assumptions we can use in the modelling of the real nebular objects. The ionizing radiation transfer problems and their solutions are considered in details. The modern approach to the finding of the optimal photoionization models of the nebular objects proposed by author is briefly described.

The comparison analysis of the different modern approaches for the determination of the energy distribution in the ionizing radiation spectrum is briefly overwiewed in Section 6. The method independent on assumptions above ionizing source nature is considered in details.

The coupled using of the optimized photoionization modelling with the ionizing radiation spectrum determination and diagnostic methods for the investigation of the Lyc-spectrum transformation in the stellar wind bubble is demonstrated in last section.

2 Nebular Objects

2.1 History of the Discovering and First Observations

In the book *Almagest* by Claudius Ptolemaeus (Ptolemy) (around A.D. 150) the five stars noted that appeared nebulous. Also in this book the region of nebulosity between the constellations Ursa Major and Leo that was noted as not associated with any star.

The first recorded observation of nebula (by naked eye, of course), as distinct from a star cluster, and noted "a little cloud"(as we know today it is Andromeda Galaxy) belongs to the Persian astronomer, Abd al-Rahman al-Sufi (Book of Fixed Stars (964)). In this book the Omicron Velorum star cluster, noted as a "nebulous star Brocchiś Cluster and other nebulous objects are also cataloged.

In 1054 the Supernova SN 1054, that created the Crab Nebula, was observed by Arabic and Chinese astronomers in 1054. We donť know why, but al-Sufi did not note the Orion Nebula, which is at least as prominent as the Andromeda galaxy in the night sky. Therefore, the Orion Nebula was discovered using a telescope only in November 26, 1610 by Nicolas-Claude Fabri de Peiresc The first detailed study of the Orion Nebula was performed in 1659 by Christian Huygens.

In 1715 Edmund Halley published a list of six nebulae. In 1746 Jean-Philippe de Cheseaux compiled a list of 20 nebulae (including eight not previously known). From 1751, Nicolas Louis de Lacaille cataloged 42 nebulae from the Cape of Good Hope, with most of them being previously unknown. In 1781 Charles Messier compiled a catalog of 103 nebulae [1]. It is necessary to say that Charles Messier in 1764 in their above catalog of nebulous object listed as M27 the Dumbbell Nebula in the constellation of Vulpecula. It was the first discovered planetary nebula. Planetary nebulae are faint objects in the night sky, they are invisible to the naked eye. Therefore, there was no chance to discover these objects without using telescopes . Early observers were working with low-resolution telescopes. Thus, M27 and subsequently discovered planetary nebulae somewhat resembled the giant planets like Uranus. William Herschel, discoverer of Uranus, eventually coined the term 'planetary nebula' for them, although, as we now know, they differ from planets.

More detailed historical review you can find, for an example, at Wikipedia (*http://en.wikipedia.org/wiki/Diffuse_Nebulae* and references therein).

William Herschel observed the Orion Nebula in 1774, and described it later as "an unformed fiery mist, the chaotic material of future suns" [2].

In 1786 William Herschel and his sister Caroline Herschel published their Catalogue of One Thousand New Nebulae and Clusters of Stars. In 1789 a second catalog of thousand objects was published. The third and final catalog of 510 objects appeared in 1802.

During long time William Herschel believed that most of nebulae were unresolved clusters of stars. But in 1790 he discovered a star surrounded by nebulosity and concluded that this was a true nebulosity, rather than a more distant cluster [1].

2.2 Spectroscopic Analysis

The nature of nebulae was unknown until the first spectroscopic observations were made in the mid-19th century.

William Huggins was one of the earliest astronomers to study the optical spectra of astronomical objects used a prism to disperse their light The first spectroscopic analysis of nebulae was done in 1864 by William Huggins (assisted by his wife Mary Huggins). Some of them, such as Andromeda Nebula, had spectra quite similar to those of stars (as we now know, they are galaxies consisting of hundreds of millions of individual stars). Others looked very different. Orion Nebula and other similar objects showed only a small number of emission lines.

In August 29, 1864, Huggins was the first to take the spectrum of a planetary nebula when he analyzed NGC 6543 (Cat's Eye Nebula). Cat's Eye Nebula and other similar objects showed only a small number of emission lines. The brightest of these was at a wavelength of 500.7 nanometres, which did not correspond with a line of any known element. At first it was hypothesized that the line might be due to an unknown element, which was named Nebulium – a similar idea had led to the discovery of helium through analysis of the Sun's spectrum in 1868. However, while helium was isolated on Earth soon after its discovery in the Sun spectrum, Nebulium was not. In the early 20th century, Henry Norris Russell proposed that rather than being a new element, the line at 500.7 nm was due to a familiar element in unfamiliar conditions. The rest shown a continuous spectrum and thus, it was concluded that these objects consist of many stars.

In 1912 Vesto Slipher shown that the spectrum of the nebula surrounding the star Merope matched the spectra of the Pleiades open cluster. Thus, the nebula radiates by reflected star light.

Slipher and Edwin Hubble continued to collect the spectra from many diffuse nebulae, finding 29 that shown emission spectra and 33 had the continuous spectra of star light. In 1922, Hubble announced that nearly all nebulae are associated with stars. He also discovered that the emission spectrum nebulae are nearly always associated with stars having spectral classifications of B1 or hotter (including all O-type main sequence stars), while nebulae with continuous spectra appear with cooler stars. Both Hubble and Henry Norris Russell concluded that the nebulae surrounding the hotter stars are transformed in some manner.

For more detailed information (references, images of nebulae) see, for an example, *http://en.wikipedia.org/wiki/Planetary_ nebula.html*, *http://en.wikipedia.org/wiki/H_ II_ region*, *.../wiki/Diffuse_ Nebulae*.

2.3 Forbidden Lines and Nebulium problem solution. Types of nebulae.

In the 1920s it was shown that in gas at extremely low densities electrons can populate excited metastable energy levels in atoms and ions. At higher densities are rapidly de-

excited by collisions [3]. Electron transitions from these levels in doubly ionized oxygen give rise to the 500.7 nm line [4]. These spectral lines, which can only be seen in very low density gases, are called forbidden lines. Spectroscopic observations thus, showed that planetary nebulae consisted largely of extremely rarefied ionized oxygen gas (OIII).

In high-density gas atom/ion levels population defined mainly by collisions, and we can determine these populations assuming local thermodynamical equilibrium (LTE). In low-density gas averaged time between collisions is larger than electron life-time at atom/ion energy level (even if this level is metastable). Therefore, nebular plasma is highly non-LTE (NLTE) enviroment. To the energy levels population we must use statistical equilibrium equations system.

For example, the mean density of the gas in the plane of our galaxy at the solar radius is about 0.3 cm^{-3}. Density in a molecular cloud is much higher – about $10^6 cm^{-3}$. But this is completely negligible compared with the density encountered in the Earth's atmosphere ($\approx 2 \times 10^{18} cm^{-3}$).

The astrophysical low-density NLTE plasma with electron temperature sufficient to metastable level population by electron-ion colissions we will call nebular object.

Nebular objects can be classified in following major groups.

A giant H II region is a large cloud of gas and ionized gas of glowing low density in which star formation has recently taken place. Young, hot, blue stars formed from and into the gas emit large amounts of ultraviolet photons, ionizing and heating the gas surrounding them. H II regions have sometimes several hundred light-years across and are often associated with giant molecular clouds in which star formation takes place. These giant molecular clouds contain of protostar which after transformation in the stars produce the H II region in surrounding gas. The first known H II region was the Orion Nebula. H II regions contain large amount of ionized atomic hydrogen. Therefore, they are referred to as H II by astronomers (H I region means neutral atomic hydrogen, and H_2 means molecular hydrogen). H II regions have extremely diverse morphologies, because the distribution of the stars and gas inside them is inhomogeneous. H II regions may contain thousands of stars. Massive stars explosions (supernova) at the end of their life and strong stellar winds from the most massive stars cause gases dispersion of the H II region, leaving behind a cluster such as the Pleiades. Some H II regions are observed at very large distances in the Universe – in other galaxies. They are so-called an extragalactic H II regions. Determination of physical characteristics and chemical compositions in such objects is important for an investigation of the distance and chemical evolution in other galaxies. Spiral and irregular galaxies contain a lot of H II regions. H II regions in the spiral galaxies, including the Milky Way, are concentrated in the spiral arms. In the irregular galaxies they are distributed chaotically. Some galaxies contain huge H II regions, which may contain tens of thousands of stars. Examples include the 30 Doradus region in the Large Magellanic Cloud and NGC 604 in the Triangulum Galaxy. Giant H II regions are main part of blue compact dwarf galaxies, which are characterized by active stars formation processes and low-metallicity (low abundance of elements heavier than He). Study of physical characteristics and chemical compositions in these H II regions is very useful in determination of prymordial helium (amounts of helium synthesied during Big Bang Nucleosynthesis) and its enrichment during stellar chemical evolution of matter.

Diffuse emission and reflection nebulae. Most nebulae can be described as diffuse nebulae. It means that they are extended and contain no well-defined boundaries. In

visible light these nebulae may be divided into emission nebulae and reflection ones. It depends on emitted photons that come from the nebula. Emission nebulae consist of ionized gas (mostly ionized hydrogen) that produces spectral line emission.

Active Galactic Nuclei. Many galaxies show characteristic nebular emission lines in the spectra of their nuclei [5]. In most of these objects, the gas photoionization is caused mainly by hot stars in the nucleous, and correspondingly they are much like a giant H II regions or clusters of H II regions (so called starburst galaxies). But small fraction (a few percents) of all spiral galaxies have ionized gas in their nuclei emitting an emission-line spectrum with a wider range of ionization than any H II region [5]. Also, usually emission-line profiles in spectra of these galaxies nuclei correspond to a significantly greater range of velocity than in starburst galaxies. These galaxies are called Seyfert galaxies. There are many of the most luminous radio galaxies that have nuclei with very similar emission-line spectra. Also, quasars (quasistellar radio source) and QSO (quasistellar objects) are radio-loud and radio-quiet analogues of Seyfert galaxies [5]. All these objects are called active galactic nuclei. Much of the ionized gas in active galactic nuclei is photoionized. However, the main source of the ionizing radiation is not a hot stars, but probably accretion disc around a central massive black hole, or/and relativistic particles and, perhaps, magnetic field associated with immediate environs of the black hole [5].

Planetary nebulae are an emission nebulae that consist of an expanding shell of ionized gas and dust ejected during the asymptotic giant branch phase of certain types of stars at the late stage in their life. They are a relatively short-lived phenomenon, lasting a few tens of thousands of years, compared with a typical stellar lifetime of several billion years. At the end of the star's life, during the red giant phase, the outer layers of the star are expelled via pulsations and strong stellar winds. Without these opaque layers, the hot, luminous core (white dwarf) emits ultraviolet radiation that ionizes the surrounding ejected nebula. Ionizing quanta cause photoionization processes in nebula which increase electron temperature to 10000-20000^{o}K. The nebula transforms high-energy ultraviolet (UV) quanta into larger amount of low-energy infrared, optical and UV quanta. This energized nebula radiates as a planetary nebula. Planetary nebulae play a crucial role in the chemical evolution of the galaxy, returning material to the interstellar medium that has been enriched with heavy elements and other products of nucleosynthesis (such as carbon, nitrogen, oxygen and calcium). In more distant galaxies, planetary nebulae may be the only objects that can be resolved to yield useful information about chemical abundances. In recent years, Hubble Space Telescope images have revealed many planetary nebulae to have extremely complex and varied morphologies. About a fifth are roughly spherical, but the majority are not spherically symmetric. The mechanisms which produce such a wide variety of shapes and features still are not well understood, but binary central stars, stellar winds and magnetic fields may all play a role.

Supernova remnant is the structure resulting from the explosion of a massive star as Supernova. Such structure is bounded by an expanding shock wave, and consists of ejected material expanding from the explosion, and the interstellar material it sweeps up and shocks along the way. We know two possible routes to a Supernova: 1) if massive star ($>8M_\odot$)run out of fuel for generating fusion energy in its core (all elemetnts to Fe are synthesised), then star very rapidly collapses inward under the force of its own gravity to form a neutron star or a black hole, and other shells of star which contain amount

of exothermical fuel (nuclei of elements less massive than Fe) ; 2) if a white dwarf star, accumulating by accretion material from a companion star, reaches a critical mass, then it undergoes a thermonuclear explosion. In both cases the Supernova explosion will be occured. Supernova expels much (in the first above case) or all (in the last case) the stellar material with velocities as much as 10% the speed of light (about 30,000 km/s). When this material collides with the surrounding circumstellar or interstellar medium, it forms a shock wave that heats the plasma up to temperatures above millions of K. The shock continuously slows down over time as it sweeps up the ambient medium, but it can expand over hundreds of thousands of years and over tens of parsecs before its speed falls below the local sound speed. Most famous and best-observed young Supernova remnant was formed by SN 1987A. It was a Supernova in the Large Magellanic Cloud that appeared in 1987 (it exploded approximately 168,000 years ago, because of finite light speed). Other well-known Supernova remnants are Tycho (SN 1572), named after Tycho Brahe who recorded the brightness of its original explosion, and Kepler (SN 1604), named after Johannes Kepler. Probably, most famous Supernova remnant is Crab Nebula. It is remnant from Supernova that appeared in 1054 and observed by Chinese and Arab astronomers. In the Crab Nebula the non-thermal synchrortron spectrum is observed from the radio- to optical-frequency region. Extrapolation of this spectrum in ultraviolet frequency region (ionizing radiation) indicates that this synchrotron radiation is probably source of the ionizing radiation photons. Thus, there are three types of Supernova remnant: 1) shell-like, such as Cassiopeia A; 2) composite, in which a shell contains a central pulsar wind nebula, such as G11.2-0.3 or G21.5-0.9; 3) mixed-morphology (also called "thermal composite") remnants, in which central thermal X-ray emission is seen, enclosed by a radio shell. The thermal X-rays are primarily from swept-up interstellar material, rather than supernova ejecta. Examples of this class include the SNRs W28 and W44 (W44 additionally contains a pulsar and pulsar wind nebula; so it is simultaneously both a "classic"composite and a thermal composite).

Nova remnant. If binary stellar system has one companion white dwarf and second star that overflows its Roche lobe, then the white dwarf will steadily accrete gas from the companion's outer atmosphere. The white dwarf consists of degenerate matter, and it does not inflate at increased heat. The accreted hydrogen is compressed upon white dwarf surface. The hydrogen fusion rate depends on temperature and pressure. When surface is compressed hydrogen heats to a temperature of some 20×10^6 ^{o}K, then nuclear fusion reaction occurs. The hydrogen burning is thermally unstable (stable hydrogen fusion can occurs on the surface only for a narrow range of accretion rates) and rapidly converts a large amount of the hydrogen into other heavier elements in a runaway reaction. The enormous amount of energy liberated by this process blows the remaining gases away from the white dwarf's surface and produces an extremely bright outburst of light. The rise to peak brightness can be very rapid or gradual. It depends on the speed class of the Nova. After the peak, the brightness declines steadily. The amount of material ejected in novae is usually only about 1/10000 of a Solar mass. It is quite small relative in comparison to the mass of the white dwarf. Therefore, many recent novae are surrounded by faint and small shell, which irradiate emission-line spectra.

Dark nebulae are similar to diffuse nebulae, but they are not seen by their emitted or reflected light. Instead, they are seen as dark clouds in front of more distant stars or in front of emission nebulae. These nebulae are out of the aim of this book, because of

in these objects no ionizing radiation.

For more detail information, references, and nebulae images see, for an example, *http://en.wikipedia.org/wiki/Diffuse_ Nebulae*, *http://en.wikipedia.org/wiki/Supernova_ remnant*, *.../wiki/Nova.html*.

3 Determination of the electron temperature and density using diagnostic ratios between emission line intensities

3.1 Diagnostic ratios between emission line intensities for the electron temperature determination

If some ions have energy-level structure that results in emission-lines from two different upper levels with considerably different excitation energies in the observable wavelength region, then ratios between intensities of such lines are very sensitive to electron temperature. Let consider, for an example, the energy levels diagram of [O III] ion (see Fig. 1 a). The transition resulting [O III] λ4363Åemission-line occurs from the upper ^1S level, while λ4959Åand λ5007Ålines occur from the intermediate ^1D level. Relative rates of excitation to the ^1S and ^1D levels depend very strongly on electron temperature. Therefore, the relative strength of the lines emitted during transition from these levels can be used to determination of electron temperature. Similar energy-level structure have others ions, such as [NII] $\lambda5755/(\lambda6548+\lambda6583)$, [Ne III] $\lambda3343/(\lambda3869+\lambda3968)$, [S III] $\lambda6312/(\lambda9532+\lambda9069)$. These ratios are also used in the electron temperature determination. Corresponding expressions can be found, for an exapmle in book [5]. Temperature diagnostic ratios between emission line intensities have strong exponential dependece on electron temperature and very weak dependence on electron density.

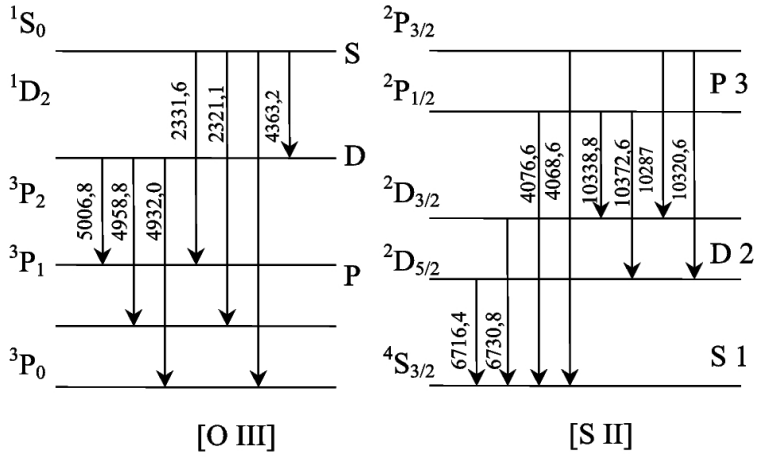

Рис. 1: The energy-level diagram for lowest terms of ion [OIII] and for $3p^3$ configuraion of ion [SII]

3.2 Diagnostic ratios between emission line intensities for the electron density determination

Ratios between two emission-line intensities of the same ion, emitted by different levels with nearly the same excitation energy, may be useful for the average electron density determination in nebular objects. For such levels the relative excitation rates depend only on the ratio of collisional strengths. If two levels have different radiative transition probabilities or different collisional deexcitation rates, then the relative populations of these two levels depend on the electron density in nebula. Therefore, the relative strength of the lines emitted during transition from these levels may be used in electron density determination. Let consider, for an example, the energy levels diagram of [S II] ion (see Fig. 1 b). In the low-density limit the collisional excitation (by free electron) is followed by emission of photon, and corresponding relative rates the $^2D_{3/2}$ and $^2D_{5/2}$ levels are proportional to their statistical weights. Therefore, the relative ratio strengths of the corresponding emission lines (in our case λ6716Å/λ6731Å) is constant. In the high-density limit collisional excitation and deexcitation dominate and defined by a Boltzmann populations ratio, and the relative ratio strengths of the two above lines also are constant, but with some different value, than in low-density limit (see in more details [5]). The transitional density region between low- and high-density limits occurs in the neighborhood of the critical density. Detailed variation of intensities ratio with the electron temperature can be obtained from the full solution of the statiscial equilibrium equations, which also take into account all transitions in the above energy levels diagram, including excitaion to the $^2P^0$ levels with subsequent cascading downward. The similar energy-level structure have others ions, such as [OII] (λ3729/λ3726), [N I], [Cl III], [Ar IV], [K V], [Ne IV] (λ2422/λ2424). You can find more detailed information in book [5].

3.3 Overview of the various diagnostic methods.

T_e-method and two zones model. T_e method is based on the temperature diagnostic ratios between emission line intensities and mainly was used for oxygen abundance determination in H II regions. Pagel et al. [7] proposed two-zones model for oxygen abundance determination in H II regions. All main expressions for this method can be found in [6]. At the beginning, the electron temperature in zone [O III] is determined using [O III] $\lambda4363/(\lambda4959+\lambda5007)$ temperature dignostic ratio. Then, temperature in zone [O II] is calculated using it's approximation dependence on electron temperature in zone [O III]. Last dependence is obtained from photoionization models grid of H II regions. Using electron temperatures in both zones, the relative ionic abundance, O^{++}/H^+ and O^+/H^+ are calculating on the base of observed relative (to H_β) line intensities of [O III] and [O II]. Of course, for full oxygen abundance determination we need to correct unbserved ionization stages. But, frequently, for this purpose the simple expression $O/H=O^{++}/H^+ + O^+/H^+$ is used. Of course, it is not very good way for precise oxygen abundance determination in all H II regions (see next Section below). The electron density is mainly determined using electron density diagnostic ratios or assuming some low value, because of the weak dependens of electron temperature diagnostic ratio on density. The similar approaches are used for nitrogen and sulfur chemical abundances determination.

R23 and P methods. Frequently, flux in emission line [O III]λ4363Åis not available from observations. In such cases T_e method can not be used. Pagel et al. [8] developed R_{23}-method, that uses only strong oxygen lines. The parameter R_{23} is defined as $R_{23} = (I_{[\mathrm{O\ II}]\lambda3726+\lambda3729} + I_{[\mathrm{O\ III}]\lambda4959+\lambda5007})/I_{H\beta}$, where each of $I_{...}$ is the intensity of the corresponding lines. This method allows determine relative oxygen abundance, O/H, directly from observed relative intensities of strong oxygen lines. For this purpose many calibration dependences O/H – R_{23} were obtained using results from T_e-method and photoionization modelling [9–11]. Such dependences have two solutions – for values of $12 + \log(O/H)$ higher and lower than of 8.2 correspondingly. Calibration, proposed by Edmunds and Pagel [10], is most frequently used. Also, widely used calibration is from [12]. If photoionization modelling is used to some calibration derivation, then this calibration depends on modelling assumptions. There are not a great amount of H II regions in spiral galaxies with observed [O III]λ4363Å emission line. Thus, T_e-method is not very useful for above calibration derivation. But, even in T_e-method the correction for unobserved ionization stages is required for precise O/H determinaion. The error of obtained oxygen abundance is large, because of the calibration dependences O/H – R_{23} dispersion. Therefore, for the most precise abundance determination the P-method was proposed by [13, 14], where excitaion parameter, P, is defined as $12 + \log(\mathrm{O/H})_P = \frac{R_{23}+54.2+59.45P+7.31P^2}{6.07+6.71P+0.37P^2+0.243R_{23}}$, where $R_{23} = R_2 + R_3$, $R_2 = \frac{I_{[\mathrm{O\ II}]\lambda3727+\lambda3729}}{I_{\mathrm{H}\beta}}$, $R3 = \frac{\mathrm{I}_{[\mathrm{OIII}]\lambda4959+\lambda5007}}{I_{\mathrm{H}_\beta}}$, and $P = R_3/R_{23}$. Thus, in P-method for every of P-parameter values corresponds separate O/H – R_{23} dependence.

Methods of full diagnostic use all (or most of all) available from observations diagnostic ratios between line intensities [15,16]. For an example, let consider the code DIAGN [15], that is one of computer realise of full diagnostic methods. Most of the observed diagnostic ratios have strong dependence on both the electron temperature and density. For every of such ratios observed value the dependence electron temperature on electron density, $T_e - n_e$, can be derived. The energy level populations are calculated as solution of statistical equlibrium equations for 5-levels structure. The crossing of $T_e - n_e$ dependences for different observed diagnostic ratios defines the T_e and n_e values in observed nebular object. All of diagnostic ratios may be related to the four different ionization zones, so in each of these zones the T_e and n_e values can be derived, if observation gives available enough number of diagnostic ratios. In most cases the crossing of third and more $T_e - n_e$ dependences is not in one point, they rather bound the $T_e - n_e$ area. The value of this area depends on the errors in atomic data, and, on the another hand, on the electron density fluctuations in nebula. The T_e and n_e values in corresponding zone are selected from above area by user. These values are used in ionic abundances determination from most of all observed emission lines. If the expressions for ionization-correction factors are available, then they can be used to the correction for unobserved ionization stages and, correspondingly, for the chemical composition determination of corresponding chemical elements. The similar realization of the full diagnostics method can be found in the IRAF task *temden* of the package *nebular* [16].

4 Determination of the chemical composition in nebular objects

Observed data does not have available emission lines of all ionization stages of the corresponding ion. Therefore, for the chemical abundance determination a chemical element the sum over all ionic abundances, obtained from observation using diagnotic methods, must be corrected for unobserved ionization stages. Frequently, for this purpose, the ionization-correction factors (ICFs) are using. For an example, if A/H means full chemical composition of element A relative to hydrogen (H) abundance, and A^{+i}/H^{+} is relative ionic abundance of element A in ionization stage i, then $\frac{A}{H} = ICF(A, A^{+i}) \times \frac{A^{+i}}{H^{+}}$. In this case the chemical composition, A/H, are derived from observed ionic abundance (obtained using diagnostics method), A^{+i}/H^{+}, using corresponding ionization-correction factor, ICF(A,A^{+i}).

In this section main approaches to the chemical composition determination are considered.

4.1 Empirical ionization-correction factors.

If two ions of different chemical elements have near values of ionization potentials, and emission line(s) of one of these ions is (are) observed, and the second one ion is not presented in observed spectrum, then in this approach the data of observed ion may be used for the correction of the above corresponding ionization stage. But, such approach does not take into account the differences between photoionization cross sections of the above two ions. Therefore, empirical ICFs are not precise in most cases.

4.2 Derivation of ionization-correction factors from photoionization modelling results

Presence of unobserved ionization stages are caused mainly by narrow observed spectral wavelength region and also by low strength of the corresponding ion emission lines. To avoid of these problems the photoionization modelling can be used. The main aim of the photoionization modelling is to derive spectrum of the nebular objects on the base of input chemical composition, ionizing spectrum, character of density distribution. Model calculates ionizing radiation transfer through nebular object, taking into account all important physical processes in nebular plasma, caused by the photoionization. Thus, the chemical compositions are defined as input parameters, and model calculates of all assumed ions abundance along corresponding direction.

There are two approaches for derivation of expressions for ICFs from photoionization modelling results. In both cases the photoionization models grid over input parameters values in range that are specified for nebular objects class (planetary nebulae, or H II regions, for an example) must be calculated.

In the first approach the ionic abundances obtained from grid calculations and averaged over model volume are used. Assumed chemical compositions are used for the derivation of the expressions for ionization correction factors. This approach was used, for an example, in [17]. Such ICFs combined with ionic abundances obtained using above diagnostic methods are usually used for chemical composition determination in

real nebular objects. But, averaged over volume (or radius) ionic abundances are not the same as corresponding ones, obtained using diagnostic method(s) [18]. It is because in diagnostic methods the T_e, n_e, and ionic abundances values by default (or by basic assumption) are the same over all volume of the ionization zone, while from photoionization modelling the distribution of ionic abundances over modelling nebula volume are obtained, and averaging procedure is used to the determination of one abundance value for corresponding ion instead of values distribution.

The predicted modelling spectra are very reach and are obtained in the wide wavelength range in comparison with observed ones. Therefore, in the second approach [18–21] the modelling spectra are used "as observed"in diagnostic methods like DIAGN (see previous section). Obtained in this way ionic abundances from all grid models cobined with assumed chemical compositions in photoionization models grid are used to the derivation of the expressions for ICFs. We used this approach for the chemical composition determination in low-metallicity H II regions in blue compact dwarf galaxies [18, 19] and planetary nebulae [20, 21]. This approach also allows to test precision of the every derived ICFs as well as other ICFs. For this purpose, the model chemical composition of the corresponding chemical element is calculated using each of obtained corresponding ICFs and data on ionic abundances obtained from photoionization modelling. The result value is compared with corresponding abundance assumed in model. ICFs with errors less than 10% were used to the chemical composition determination in low-metallicity H II regions and Galactic planetary nebulae. At present we are using this approach to the derivation of ICFs for high-metallicity H II regions, low-metallicity planetary nebulae, and supernovae remnants.

4.3 Direct derivation of chemical composition from optimized photoionization modelling

The photoionization modelling results (for an example, spectrum and size of the nebula) can be compared with corresponding observed data, while input model parameters (see previous subsection) are unknown. Therefore, for correct modelling of the nebular object (or some volume part), we need to use the procedure for optimal photoionization model search. We call this search process as 'optimized photoionization modelling' [22–26]. The main task of above optimization procedure is to find optimal photoionization model for corresponding nebular object with values of fluxes in emission lines and size of the ionized region that are closest to the observed ones, using variation of the main input parameter. In result the optimal values of model input parameter should be obtained. More detailed description of optimized photoionization modelling can be found below in last subsection of the following section.

The abundance of most of chemical elements are varied separately. It is in contradiction with most grid modelling, where such parameter as metallicity (single normalization parameter for all heavy elements abundances) was frequently used for simplicity. Thus, the chemical compositions of elements are determined in optimized photoionization modelling in independent on ICFs way. The optimizer (optimization procedure) finds the optimal photoionization model for one real nebular object, and for this purpose it frequently calculates many thausends photoionization models. It requires long time. Thefore, the chemical compositions, obtained from optimal photoionization modelling,

can be used in future to the correction of the corresponding ICFs results.

5 Photoionization modelling of the nebular objects

The diagnostic methods assume that electron themperature and density as well as ionic abundances are the same over all volume of the ionization zone. But it is not correct for real nebulae, because gas distribution is inhomogenious and frequently there are many ionizing sources (for an example, in the case of giant H II regions). Even in ideal spherical-symmetrical case with central ionizing source (star, or stars cluster) above parameters as well as ionic abundances have different values along radius, because of ionizing radiation transfer with absorption and emission of ionizing quanta in nebula. Therefore, for more detailed investigation of the nebular objects we need to obtain their photoionization models.

In this section the main steps of the photoionization modelling algorithms are considered.

5.1 Basic equations

The basic equations for photoionization modelling of the nebular objects can be divided into three groups [27]:

1) Hydrodynamic equations of motion. Let consider these equations in Eulerian reference frame, and in the forms of conservation laws. The first one is the mass conservation (or continuity) equation,

$$\frac{\partial \rho}{\partial t} \; + \; \nabla(\rho \mathbf{v}) \; = \; 0, \tag{1}$$

where ρ is the mass density, t is the time, and $\mathbf{v}$ is the velocity vector. The second one is the momentum equation:

$$\frac{\partial (\rho \mathbf{v})}{\partial t} \; + \; \nabla(P + \rho \mathbf{v^2}) \; = \; \mathbf{g}\rho, \tag{2}$$

where P is the gas pressure, $\mathbf{g}$ is the acceleration caused by gravity, magnetic filed, and/or light pressure. The third law represents the energy conservation:

$$\frac{\partial}{\partial t}\left[\rho\left(E + \frac{v^2}{2}\right)\right] \; + \; \nabla\left[\rho \mathbf{v}\left(E + \frac{v^2}{2}\right) + P\mathbf{v}\right] \; = \; \mathbf{v}\;\mathbf{g}\rho \; + \; H \; - \; C, \tag{3}$$

where E is the internal kinetic energy per unt mass ($E = U/\rho$, where U is the full internal kinetic energy), H and C represent the functions of the gas heating and cooling corresondingly per unit volume per unit time due to the atomic processes. The gas pressure is given by the quation of state, the relationship between pressure, density, and temperature (T): $P \; = \; \frac{\rho k_B T}{\mu m_H} = n_{total} k_B T$. Frequently, the radiation pressure can be neglected. For the pressure there are two limiting cases [5]. The first one, is if the balance between heating and cooling processes in nebular region determines the temperature, then the pressure depends on the temperature almost linearly. The opposite (adiabatic) case is when radiation losses in nebular gas can be neglected, then the internal energy

of the gas is conserved. In the last case pressure depends on the density as $P = C\rho^{\gamma}$, where $\gamma = 5/3$ for monoatomic gas, while $\gamma = 7/5$ for diatomic gas.

It must be noted, that if nebular object consists of the gas and dust, then momentum eqution(s) should be written for each above component. These equations must contain detailed description of the collission processes between particles of the diferent components.

2) Equation for radiation transfer describes the behavior of the radiation intensity, $I_\nu(\mathbf{n}, \mathbf{r})$, with frequency, ν, in the dependence on the position, $\mathbf{r}$, and the direction, $\mathbf{n}$ [27]:

$$\frac{1}{c}\frac{dI_\nu}{dt} + \mathbf{n}\nabla I_\nu = j_\nu - \kappa_\nu I_\nu, \tag{4}$$

where c is the light speed, j_ν and κ_ν are the coefficient of the emissivity and absorption of the nebular gas at frequency, ν.

Also, the average intensity and flux over solid angle, Ω, are usually used: $J_\nu = \frac{1}{4\pi}\int_{4\pi} I_\nu d\Omega$, $\mathbf{F}_\nu = \int_{4\pi} \mathbf{n} I_\nu d\Omega$.

Transition equations, describing the evolution of the particles density, which are in state i, may be written [27] as

$$\frac{dn_i}{dt} + \nabla(n_i \mathbf{v}) = G_i + \sum_{j\neq i} R_{j\to i} n_j - n_i \left(S_i + \sum_{j\neq i} R_{i\to j} \right), \tag{5}$$

where $R_{j\to i}$ and $R_{i\to j}$ represent the transition coefficients between states i and j; G_i and S_i are the gain and loss correspondingly of the state i due to the other physical processes. This form of transition equations may be used for description of the transitions between energy levels of atom, ion, molecule or dust grain. Also, this form may be initial to the derivation of the ionization balance equations, that allow to determine the ionic abundances in different ionization stages. The above cofficients from equation (5) depend on the local ionizing radiation field, the electron density and temperature as well as others physical parameters, that characterise the local state of the gas in a nebula.

5.2 Static, stationary, and non-stationary models

The most simple case of photoionization modelling is the static one. Static models exclude the gas dynamics. It means that in the all basic equations the velocity as well as the derivates over time are also equivalent zero. So, all terms of the equation (1) are equivalent zero; the equation (2) becomes the equation of the hydrostatic equilibrium (it transforms to the equation $P = const$). The energy balance equation (3) is simplyfied to $H = C$, and transition equations (5) becomes the equation systems of the ionization-recombination and statistical equlibrium.

In most nebulae the main heating source is a photoionization, because it causes the emergence a lot number of free fast electrons. Thus, energy that comes in unit volume per unit time from photoionizations of the all taken into account ions X^i can be determined as follows:

$$H_{phot}(\mathbf{r}) = \sum_{X^i} n(X^i, \mathbf{r}) \int\limits_{\nu_0(X^i)}^{\infty} \frac{\int_0^{4\pi} I_\nu(\mathbf{r}, \Omega) d\Omega}{h\nu} \sigma_{phot}(\nu, X^i)\, h(\nu - \nu_0(X^i)) d\nu. \tag{6}$$

Here, integrating is starting for each of ions at corresponding for this ion the ionization potential frequency ν_0. The cooling rate $C = \Lambda_{cl} + \Lambda_{ci} + \Lambda_{rec} + \Lambda_{ff}$ for nebular medium includes cooling by collisional excitation (Λ_{cl}) and ionization (Λ_{ci}) as well as by recombinations (Λ_{rec}) and free-free radiation (Λ_{ff}).

It is required to ensure, that assumption about energy balance in modelling nebular object is right. For this purpose, the time scale for arising the thermal balance equilibrium should be calculated: $t_T \sim \frac{n_e\, kT_e}{C}$, For conditions in planetary nebulae ($n_e \sim 10^3 cm^{-3}$, $T_e \sim 10^4$K) the value $C \sim 10^{-17} erg \cdot cm^{-3} \cdot\ c^{-1}$, and, therefore, $t_T \sim 10$ years. Because $C \ll n^2$, this time scale will be lower for young planetary nebulae. Thus, planetary nebulae envelopes in most cases are in thermal equilibrium, because of comparable larger age. H II regions have on order lower density, and it is because t_T values for them is on order higher ($t_T \sim 100$ years). But, age of most H II regions is much higher than above value. Therefore, for most H II regions the energy balance assumption can be used. Before such modelling it is required to ensure, that in apperture the shock wave front was not observed, of course. In opposite case the heating from shock must be taken into account.

The ionization-recombination equilibrium may be written as

$$n^*_{ion}(X^i, \mathbf{r}) + n^d_{ion}(X^i, \mathbf{r}) + n^c_{ion}(X^i, \mathbf{r}) + n^{ch}_{ion}(X^i, \mathbf{r}) = n^{rad}_{rec}(X^{i+1}, \mathbf{r}) + n^{di}_{rec}(X^{i+1}, \mathbf{r}) + n^{ch}_{rec}(X^{i+1}, \mathbf{r}), \tag{7}$$

for all taken into account ions, X^i ($i-$ represents the ionization stage). Here, on the left side, $n^*_{ion}(X^i, \mathbf{r})$, $n^d_{ion}(X^i, \mathbf{r})$, $n^c_{ion}(X^i, \mathbf{r})$, $n^{ch}_{ion}(X^i, \mathbf{r})$ correspond to the number of the ionizations in unit volume in vicinity of the point with coordinates $\mathbf{r}$ per unit time due to the direct and diffuse ionizing radiation, electron collision, and charge transfer correspondingly. On the right side, $n^{rad}_{rec}(X^{i+1}, \mathbf{r})$, $n^{di}_{rec}(X^{i+1}, \mathbf{r})$, $n^{ch}_{rec}(X^{i+1}, \mathbf{r})$ correspond to the number of recombinations in unit volume in vicinity of the point with coordinates $\mathbf{r}$ per unit time due to the radiative, dielectronic, and charge transfer processes correspondingly. There are enumerated all main elementary processes in most nebular objects. But, of course, sometimes additional processes should be included in above system. For an example, in a case of accretion disk in AGN the Compton scattering process becomes important.

The important equations system is the stationarity one for levels population (or, in an other words, statistical equlibrium equations system). For instance, such equation for collisionaly excited levels becomes

$$\sum_{i=1}^{j-1} n_i\, b_{ij} + \sum_{k=j+1}^{N} n_k (A_{kj} + a_{kj}) = n_j \left(\sum_{i=1}^{j-1} (A_{ji} + a_{ji}) + \sum_{k=j+1}^{N} b_{jk} \right), \qquad \sum_{k=1}^{N} n_k = 1. \tag{8}$$

where n_i, n_j, n_k are relative populations for the corresponding levels; A_{kj} and a_{kj} are spontaneous and deexcitation transition coefficient from upper level k to the lower level j; b_{ij} corresponds to the collisional excitation coefficient; N is the number of the taken into account levels. The left and right sides of these equations describe the processes that increase and decrease correspondingly level (j) population. So, the left side of this

equations system describes the processes, which increase the level j population, while right side describes the decreasing population processes. The solution of the $N-1$ linear equations system (8) gives the relative populations $(n_1, n_2, \ldots, n_N)$ of the corresponding ion levels.

How to estimate, whether using of ionization-recombination assumption is not false in the real nebular object, that is under modelling? To answer this question the time scale for arising the equilibrium between ionization and recombination processes should be calculated, as $t_r \simeq \frac{1}{n_e \alpha(X^{i+1}, T_e)}$, where $\alpha(X^{i+1})$ is the full recombination coefficient for the ion X^{i+1}. For an example, in the case of planetary nebulae the averaged values of $n_e \sim 10^3 cm^{-3}$, $T_e \sim 10^4$K, and, therefore, the t_r value does not exceed of ~ 100 years for ions with the slowest recombination scale time. For the young planetary nebulae with $n_e \sim 10^4 - 10^5 cm^{-3}$ this time is much lower. Thus, time t_r is much lower than age of the planetary nebulae. In the case of H II regions we have averaged values of $n_e \sim 100 cm^{-3}$, $T_e \sim 10^4$K. Therefore, t_r does not exceed of ~ 1000 years for ions with the slowest recombination scale time. But, the ages of the giant H II regions are million and more years. Therefore, it can be concluded that in most of above nebular objects the assumption about ionization-recombination equilibrium is right.

Most of photoionization codes are based on static assumption, or include the static case as the most simple work option.

Nebula irradiates in the near UV, optical and infrared wavelength regions transforming by physical processes in nebular plasma the hard ionizing UV-photons at $\lambda \leq 912$Å into much greater number of non-ionizing quanta. The calculation of the static photoionization model is based on the coupled numerical solution of the equations of the ionizing radiation transfer, ionization-recombination and energy balances, as well as the statictical equilibriums equation in the each of nebula points. The equations of the ionizing transfer allow to determine the ionizing radiation fluxes in the current nebula point; the ionization-recombimation equations, written for every of the accounted ions, allow to obtain ionization fractions of every chemical element in the current nebula point; and statistical equilibriums equations allows to calculate the level populations with foolowing emissivities calculations. The emissivities volume map is required for the whole modelling emission line spectrum calculation. All these system equations are physically coupled, therefore, the calculation in each elementary volume of nebula should be performed in iterational way. Namely, the first assumption of the electronic temperature (frequently it is of $T_e^{(0)} \sim 10^4$ K) is adopted. At this value the all above equations system are solved, and then the energy balance is checking. If there is no equality between heating and cooling rates, then new assumption of T_e is selected. This iteration process is repeated until the energy balance is satisfactored.

In the case of the spherically symmetrical nebula it is required to calculate the physical conditions for each of the small spherical shells in which nebulae volume is divided, but in the case of 3D-geometry the physical conditions must be estimated in each of the elementary cubic nebula volumes.

The more detailed description of the calculation algorithms used in photoionization codes can be found in papers or in documentations on these codes. For an example, widely used G.Ferland's photoionization code is described in details in [29].

In the modern approaches to the 3D photoionization modelling the three main developing directions can be noted: 1) pseudo-3D modelling, that uses results of the many

1D-models in different directions from the nebula central point for the generation of the 3D-map (see for an example [30]); 2) modelling with detailed calculations of the diffuse radiation transfer in 3D geometry (see for an example [31]); 3) using of the Monte Carlo simulations for radiation transfer solution in 3D-geometry (see for an example [32] and references therein). There is also very useful package *Shape* for interactive 3D modeling technology: *http://www.astrosen.unam.mx/shape/index.html*.

Of course, the real objects are expanding in the vacuum and they have more complex matter dynamics. The static assumption in photoionization modelling can be used, when relaxation time scales to the arising of the ionization-recombination and thermal equilibriums in nebular objects are much shorter, than time scale for the dynamic changes.

The stationary models differ from the static ones by the presence in basic equations of the spacial gradients; the time derivates are equivalent to zero, of course. It means, that in every of the spacial points in nebular objects volume, the velocity vector has non-zero values, and these valuse may be different in different spacial points, but the field of the velocities does not changes with time.

The simplest iteration scheme for the differentiation of the equations in the stationary case was proposed in [28]. This scheme was used for the implementation of the advective photoionization modelling in widely used code CLOUDY [29]. In [28] the results of the advective photoionization modelling of the Orion nebula part. It was concluded that direct impact of the advective effects on the resulting emission line spectrum met in the case when ionization parameter is much smaller, than in the case of typical H II regions. Increasing of the temperature in partically ionized gas at ionization front is not large. As detector of the advective fronts can be used peack in electron density at the ionizing front. For this peack detection the distribution along the slit of the intensity of λ6584Å[NII] emission line can be used.

The non-stationary models are still under developing. It is because there are no (or minimal ammount of) assumptions in basic equations.

If time derivate of the some physical quantity $f(\mathbf{r}, t)$ in the Lagrangian coordinate system (that moves with the fluid in opposition to the Eulerian reference frame that is stationary), Df/Dt, then it relationships with Eulerian derivates, $\frac{\partial f}{\partial t}$ and $\mathbf{v}\nabla f$ can be written [5] as $\frac{Df}{Dt} = \frac{\partial f}{\partial t} + \mathbf{v}\nabla f$. Here the first time represets changes in f over time, while the second term represents advection (changes due to the flow of upstream material into the region).

Correspondingly to the quantity that is used instead of f the following hydrodynamic equations can be written. The first one is the momentum equation:

$$\rho \frac{D\mathbf{v}}{Dt} = -\nabla P - \rho \nabla \phi, \tag{9}$$

where P is the pressure, ϕ is the gravitational potentional of the involved stars and of the nebula itself. The second one is the hydrodynamic equation of continuity:

$$\frac{D\rho}{Dt} = -\rho \nabla \mathbf{v}. \tag{10}$$

This equation represents the mass conservation and relates the density and velocity fields. The third one is the energy equations that represents the generalization of the energy

balance equation considered above:

$$\frac{DU}{Dt} = (H - C) + \frac{P}{\rho}\frac{D\rho}{Dt} - U\nabla\mathbf{v}. \tag{11}$$

From this equation it can be seen that changing of the internal kinetic energy U can resulting 1) from the energy gain and loss per volume per time (first term of the right-hand side), 2) from the heating rate due to the compression (second term), 3) and from the dilation effect, analogous to the right-hand side term of equation (10) (last right-hand term). The last equation can rewritten in a form that includes the internal kinetic energy per unit mass E (see more detailed descibing in book [5]).

Let consider now the generaliztion of the equations for ionization-recombination balance:

$$\begin{aligned}
\frac{Dn(X^{+i})}{Dt} = \\
-n(X^{+i}) \int\limits_{\nu_{ion}(X^{+i})}^{\infty} \frac{4\pi J_\nu}{h\nu}\sigma_{phot}(\nu, X^{+i})d\nu + n(X^{+i+1})n_e\alpha_A(X^{+i}, T) \\
+n(X^{+i-1}) \int\limits_{\nu_{ion}(X^{+i-1})}^{\infty} \frac{4\pi J_\nu}{h\nu}\sigma_{phot}(\nu, X^{+i-1})d\nu - n(X^{+i})n_e\alpha_A(X^{+i-1}, T) \\
-n(X^{+i})n_e q_c(X^{+i}) + n(X^{+i-1})n_e q_c(X^{+i-1}) - n^{ch}_{ion}(X^{+i}) + n^{ch}_{ion}(X^{+i-1}) \\
-n^{Compt}_{ion}(X^{+i}) + n^{Compt}_{ion}(X^{+i-1}) - n(X^{+i})\nabla\mathbf{v}
\end{aligned} \tag{12}$$

where α_A is the total recombination coefficient of the corresponding ion; J_ν represent total intensity of the ionizing radiation, that comes in corrent nebula volume. The first term of the right-hand side of the above ionization equation represents decreasing of the ion X^{+i} number density due to the photoionization, the second one represents increasing of this quantity value due to the recombinations of the ions X^{+i+1}, the pair of the third fourth terms represent the increasing and decreasing of the number density of the ion X^{+i} due to the it photoionization and recombination of the ion X^{+i-1} correspondingly; the next terms pair of terms represent the decreaing and increasing correspondingly of the ion X^{+i} abundance due to the collisional ionization of the corresponding ions; the next terms pair describes the corresponding contributions of the charge-transfer processes; the next terms pair describes the contributions from Compton effect; and last term represents the advection contribution in ion X^{+i} number density.

Finally, we need equation of the state (see subsection "Basic Equations") that in general case have to include contribution from all nebular components.

Thus, the full equations system for non-statinary modelling of the processes in the nebular medium consist of non-linear intergro-differential equations and must be solved numerically.

The more detailed description of the different hydrodynamic motions, including shocks you can find, for an example, in books [5].

5.3 Transfer equation for the direct ionizing radiation from star

If intensity of the ionizing radiation is constant, then transfer equation 4 becomes $\mathbf{n}\nabla I_\nu = j_\nu - \kappa_\nu I_\nu$.

Most of the real nebular objects are inhomogeneous, and, in the case of giant H II regions, contain of many ionizing sources (stars) scaterred over nebula volume. Therefore, in ideal case, we have to trace path of the each of the ionizing photons from the star through it's scattering, absorption (followed by all elementary processes in plasma) and reradiation by nebular plasma to the point, where photoionization occurs due to this photon absorption. But, it is too complicate task even for supercomputers. Therefore, modern so-called 3D-codes are tracing not each ionizing photons, but rather packages of photons, and are based on the Monte Carlo simulation of such packages tracing. Detailed decription of Monte Carlo simulation 3D-code Mocassin for photoionization modelling be found in [32] and at *http://www.ast.cam.ac.uk/$\tilde{b}$e/mocassin.htm*.

Frequently, for an example, in the case of planetary nebula or compact HII region surrounding single star, the ionizing source is central and single. Similar assumption about central ionizaing source can be done in the case of giant H II regions with compact starcluster in the center, if its size is much smaller than one of the sourrounding H II region. In these cases ionizing radiation can be divided into two kinds. The first one, is the direct ionizing radiation (characterized by intensities I^s_ν) from the central ionizing source (star(s)), and the second one is the diffuse ionizing radiation (characterized by intensities I^d_ν) emitted by nebular gas.

Also, if nebula has nearly spherical shape, then we can do assumption about spherical symmetry, and then all physical characteristics depend only on the distance, r, of the currect spherical shell from the nebula center. In this case transfer equation for the direct ionizing radiation becomes $\frac{dI^s_\nu}{dr} = -\kappa_\nu I^s_\nu$, It can be seen, that nebular gas emission coefficient is absent in this equation. It is replaced by the equation of diffuse radiation transfer (see next Subsection). The optical thickness is defined as $\tau_\nu = \int_{s_0}^{s} \kappa_\nu(s')ds'$ for radiation at the frequency ν. It is dimensionless quantity that characterizes by decreasing of the radiation at the frequency ν after penetrating the nebular environment along line between points s_0 and s. After dividing of the left and right side of the above transfer equation on κ_ν, it can be written as $\frac{dI^s_\nu}{d\tau_\nu} = -I^s_\nu$. The solution of this equation is $I^s_\nu(r) = I^s_\nu(r_{in})e^{-\tau_\nu(r)}$, where $I^s_\nu(r_{in})$ corresponds to the intensity of the direct ionizing radiation at the inner radius, r_{in}, of the nebula, and $\tau_\nu(r)$ is optical thickness between inner edge and current shell of the nebula correspondingly. Absorption coefficient can be written as $\kappa_\nu = \sum_{X^i} n(X^i, r)\sigma_\nu(X^i)$, where $\sigma_\nu(X^i)$ corresponds to photoionization cross-section of the ion X^i at the frequency ν.

Intensity in the void space is unchanging, but flux does not. For an example, if radiation flux at the star surface with radius is R_*, and at the inner nebula radius r_{in} the radiation flux can be written as $F^s_\nu(r_{in}) = F^s_\nu(R_*)\left(\frac{R_*}{r_{in}}\right)^2$. Therefore, the direct ionizing radiation flux at the distance r from the nebula center can be defined as follows $F^s_\nu(r) = F^s_\nu(r_{in})\left(\frac{r_{in}}{r}\right)^2 e^{-\tau_\nu(r)}$. In result, the photoionizations number per unit volume per unit time due to the direct ionizing radiation flux in spherically symmetrical nebula

with central ionizing source can be determined as follows

$$n^*_{ion}(X^i, r) = n(X^i, r)\frac{r^2_{in}}{r^2} \int\limits_{\nu_0(X^i)}^{\infty} F^s_\nu(r_{in})\, e^{-\tau_\nu(r)}\, \sigma_\nu(X^i)\, \frac{d\nu}{h\nu}, \tag{13}$$

Integrating must be done over frequency range, where ion X^i absorbs the corresponding photons. Here, $n(X^i, r)$ is the number density of the ion X^i in the shell with radius r.

5.4 Transfer equations for the diffuse ionizing radiation

Photoionizations in nebular objects are caused also by diffuse ionization radiation, that arises as result of the recombination of the free electrons onto main lowest levels of ions H^+, He^+, He^{++}, and onto second level of He^{++}, as well as Lyman L_α (He I) and L_α (He II) quanta.

The number of these photoionization per unit volume per unit time can be determined in general case as follows

$$n^d_{ion}(X^i, \mathbf{r}) = n(X^i, \mathbf{r}) \int\limits_{\nu_0(X^i)}^{\infty} \sigma_\nu(X^i) \frac{4\pi J^d_\nu(\mathbf{r})}{h\nu}\, d\nu, \tag{14}$$

where $J^d_\nu(\mathbf{r})$ is the average intensity if the diffuse ionizing radiation at given nebula point with coordinates $\mathbf{r}$. This average intensity is defined by intensities $I^d_\nu = I^d_\nu(r, \theta, \varphi)$ of the diffuse ionizing radiation that comes from all directions (here r, θ, φ are coordinates in spherical reference system of the corresponding point of the nebula).

Detailed calculation. In the general case of the inhomogenity and amorphous nebula for the calculation of intensities $I^d_\nu(r, \theta, \varphi)$ in every nebula point (or rather in every so small volume where physical conditions can be assumed as unchanging) the radiation transfer equation for diffuse radiation should be solved:

$$\frac{dI^d_\nu(s)}{ds} = -\kappa^d_\nu(s) I^d_\nu(s) + j^d_\nu(s), \tag{15}$$

where $I^d_\nu(s)$, $\kappa^d_\nu(s)$, $j^d_\nu(s)$ are the intensity, linear absorption coefficient and emission coefficient correspondingly. The diffuse ionizing radiation propagates along some direction from the outer edge of the nebula to the current point that is separated by the distance s. The outer edge of the nebula is defined by the ionizing front. In the case of the spherically symmetrical nebula this edge has spherical shape. Thus, $I^d_\nu = I^d_\nu(r, \theta)$ is only function of the radial distance r to the given nebula point and the angle θ, because $s = s(r, \theta)$.

Numerical solution of equations (15) gives us the average intensity of the diffuse ionizing radiation for every unit nebula volume in general case, or for every spherical unit shell volume in spherically symmetrical case under condition that there are no outer (beyond nebula volume) sources of the ionizing radiation ($I^d_\nu(s = 0) = 0$): $J^d_\nu(\mathbf{r}) = \frac{1}{4\pi}\int_0^{2\pi}\int_0^{\pi} I^d_\nu(r, \theta, \varphi)\, \sin\theta\, d\varphi\, d\theta$, and in the spherically symetrical case: $J^d_\nu(r) = \frac{1}{2}\int_0^{\pi} I^d_\nu(r, \theta)\, \sin\theta\, d\theta$.

On the spot approximation (OTS) for calculation of the diffuse ionizing radiation is based on the assumption, that all diffuse ionizing quanta emitted in small (unit) nebular

volume are absorbed in this volume. This assumption is better for enviroments with larger optical depth for ionizing quanta. Also, OTS approach can be used at the the first iteration of the detailed calculation of the diffuse radiation in optically thick nebulae. In the opposite case of the optically thin nebula the good assumption for the first iteration is $J_\nu^d \approx 0$.

Because under OTS aproximation it is assumed that $dI_\nu^d/ds = 0$, the equation (15) gives: $I_\nu^d = \frac{j_\nu}{\kappa_\nu} = \frac{j_\nu}{n(H^0)\sigma_\nu(H^0)}$. Also in OTS case $I_\nu^d = J_\nu^d$ [5].

Outward only approximation. In this approximation it is assumed that diffuse ionizing radiation is propagating only in outward direction from the nebula shells. Thus, the equation for the diffuse radiation transfer (15) becomes $\frac{dI_\nu^d(r)}{dr} = -\kappa_\nu^d(r)I_\nu^d(r) + j_\nu^d(r)$. Formal solution of this equation can be written as $I_\nu^d(r) = I_\nu^d(r_{in})e^{-\int_{r_{in}}^r \kappa_\nu^d(r')dr'} + \int_{r_{in}}^r j_\nu^d(r')e^{-\int_{r'}^r \kappa_\nu^d(r'')dr''}dr'$. But for outward only approximation the first term in formal solution is equivalent to zero, because the diffuse radiation arises in the nebula ($I_\nu^d(r_{in}) = 0$) and the ionizing radiation is propagating only in outward direction. Thus, resulting solution can be witten as $I_\nu^d(r) = \int_{r_{in}}^r j_\nu^d(r')e^{-\int_{r'}^r \kappa_\nu^d(r'')dr''}dr'$.

5.5 Transfer in lines

The radiation transfer equation in plane-parallel geometry in "two-stream" approximation after the integration over the angles as well as separation of the line fluxes from underlying continuum ones, and integrating over the frequency becomes [33]

$$\frac{dF_{line}}{dr} = h\nu\left[n_u B_{ul}\int J_\nu\psi_\nu d\nu - n_l B_{lu}\int J_\nu\phi_\nu d\nu\right] + h\nu n_u A_{ul} - 4\pi\kappa_c J_{line}, \qquad (16)$$

where dF_{line} is the flux integrated on the line profile and $J_{line} = \int(J_\nu - J_c)d\nu$; A_{ul}, B_{ul}, and B_{lu} are usualy radiative (Einstein) deexcitation and excitation coefficients between upper (u) and lower (l) levels; ϕ_ν and ψ_ν are the absorption and emission normalized line profiles; κ_c is the absorption coefficient of the continuum at the line frequency.

Frequently, photoionization codes (like *Cloudy* [29], for an example) are using the escape probability formalism for solution of transfer equation in lines. Before the definition of the escape probability, let define the "Net Radiative Bracket" [33]: $\rho_{ul} = \frac{n_u(A_{ul}+B_{ul}\int J_\nu\psi_\nu d\nu) - n_l B_{lu}J_\nu\phi_\nu d\nu}{n_u A_{ul}}$. Then, equation (16) may be rewritten as following:

$$\frac{dF_{line}}{dr} = h\nu\rho_{ul}n_u A_{ul} - 4\pi\kappa_c J_{line}. \qquad (17)$$

In escape probability formalism the quantity ρ is identified with the probability $P_e(\tau_\nu) = e^{-\tau_\nu/\mu}$ (μ is the cosine of the angle between the normal and lightray) of the photon emitted at the optical depth τ from the surface to escape in a single flight [33]. In the case of the slab with finite thickness, radiation is emitted by both sides, and the total escape probability is defined as [33] $P_{tot} = \frac{P_{line}(\tau_\nu)+P_{line}(T_{tot}-\tau_\nu)}{2}$, where T_{tot} is the total optical thickness of the slab at frequency ν. For line photon with emission profile ϕ_ν without underlying continuum integration over the frequences gets: $P_{line}(\tau) = \int E_2[\tau\phi_\nu]d\nu$, where E_2 is the second order integro-exponential obtained by the angle averaging escape probability P_e. The escape probability is from the both slab sides. The right side of

the equation for ρ_{ul} in this case is reduced to the first term, and the flux in line can be easily computed if the correct expression for P_{line} is used. A good overview of the different approaches to P_{line} determination, used in codes CLOUDY [29] and XSTAR (see *http://heasarc.gsfc.nasa.gov/xstar/xstar.html*), can be found in paper [33], where also suggseted other way for calculation transfer problem in lines.

In the code TITAN authors of paper [33] used accelarated lambda iterations (ALI) method [34] for the solution of transfer equation. In this approach the operator $\mathbf{\Lambda}$ is defined as follows:

$$\int J(\tau_\nu)\phi_\nu d\nu = \mathbf{\Lambda}[S_\nu(t)], \tag{18}$$

where $S_\nu(t)$ is the source function from transfer equation in the form $\mu\frac{dI_\nu}{d\tau_\nu} = -I_n u + S_\nu$ with formal solution $J(\tau_\nu) = \frac{1}{2}\int d\mu \int S_\nu e^{-(t-\tau_n u)/\mu}\frac{dt}{\mu}$. Assumming that emission and absorption profiles are equal (so-called complete redistribution assumption that makes the line source function independent of frequency) via statistical equlibrium equations for two-level atom without an underlying continuum, the source function can be witten as [33] $S(line) = \frac{J_\nu\phi_\nu d\nu + \eta B_\nu(T_e)}{1+\eta}$, where $B_\nu(T_e)$ is the Planck function at the electronic temperature T_e; $\eta = \frac{n_e q_{ul}}{A_{ul}}\left(1 - e^{-\frac{E_{ul}}{kT_e}}\right)$; and C_{ul} is the collisional deexcitation coefficient.

The following perturbations allow use of the itertive scheme [33]:

$$\mathbf{\Lambda} = \mathbf{\Lambda}^* + (\mathbf{\Lambda} - \mathbf{\Lambda}^*);\ S_\nu = S_\nu^* + \delta S_\nu. \tag{19}$$

Here $\mathbf{\Lambda}^*$ is an aproximate $\mathbf{\Lambda}$ operator, and S_ν^* was calculated at the previous iteration. Thus, in code TITAN [33] the following iterative scheme is adopted: 1) for each layer, starting from the illuminated side, the ionization, statistical, and thermal balance equations are solved by iteration using $\int J_\nu\phi_\nu d\nu$, J_{line} and J_c from the previous iteration (in result the temperature, the opacity and the emissivity are computed); 2) after reaching of the outer side of the nebula, the transfer equation is solved using ALI method and in result $J_\nu(r)$ is computed for each layer of the whole slab; 3) the above calculations are repeated until convergence. The code TITAN can be used for modelling of the radiation transfer for hot (temperate of 10^5 to 10^6K), dense (higher than $10^{12}cm^{-3}$), and optically thick medium with Thomson thickness of the order of, or greater than, unity, illuminated by X-ray. These conditions are met in Active Galactic Nuclei and in X-ray binary.

5.6 Optimized photoionization modelling

The majority of input parameters (for an example, the ionizing radiation spectrum, density distribution, chemical composition) for photoionization modelling are unavailable directly from observations, while results of this modelling (calculated modelling spectrum, ion fractions, angular size of the ionized region) can be compared with corresponding observed data. Therefore, searching of the optimal photoionization model of the real nebular object is related to the typical inverse problem. We call this task optimized photoionization modelling. The main aim of this task is to develope fast optimized approach to find the optimal photoionization model of the nebular object. In Peter A.M. van Hoof's thesis (*http://dissertations.ub.rug.nl/faculties/science/1997/p.a.m.van.hoof/*) and in papers [22–26] different approaches to the solution of this task can be found.

In this subsection our newest multistages method for optimized photoionization modelling is described.

For the ionizing radiation spectrum representation we are using power-law $F_\nu = F_{\nu_0}\left(\frac{E_\nu}{E_{\nu_0}}\right)^\alpha$, where F_{ν_0} and F_ν are fluxes at the beginning (ν_0) and in (ν) the corresponding frequency interval; E_{ν_0} and E_ν are the energies of the quanta at the beginning and in above frequency interval; α represents the spectral index, that defines the slope of the ionizing spectrum in the corresponding frequency interval. At present, we are using dividing of the quanta energy interval beyond $\geq 1Ry$ into four energy subintervals separated by the following limits: 1) Limit $E_{\nu_0} = 1Ry$ corresponds to the ionization potential of the neutral hydrogen H^0. Also, this energy is close to the ionization potentials of the neutral oxygen O^0 ($1.001Ry$) and neutral nitrogen N^0 ($1.068Ry$). Nearby this limit is the ionization potential for iron ion Fe^+ ($1.190Ry$). 2) Limit $E_{\nu_0} = 1.8Ry$ corresponds to the ionization potential of the neutral helium He^0 and it is close to the ionization potentials of the ions S^+ ($1.715Ry$) and Ar^+ ($2.031Ry$). 3) Limit $E_{\nu_0} = 2.57Ry$ is between ionization potentials of the S^{++} ($2.56Ry$) and O^+ ($2.581Ry$). 4) Limit $E_{\nu_0} = 4Ry$ corresponds to the ionization potential of the He^+. Relatively close to this limit is the ionization potential for the ion O^{++} ($4.038Ry$). 5) Limit $E_{\nu_0} = 30.4Ry$ corresponds to the high-energy edge of the ionizing spectrum interval, that is under optimization.

At the second and fourth above limits the jumps are defined.

The aim of the optimized photoionization modelling is to find optimal values for input free parameters by the fit of the modelling results to the observed ones. The free parameters in our models are the the internal radius of the spherical or cylindrical H II region (R_{in}); the seven mentioned above fluxes defining the ionizing radiation spectrum; the total number of the ionizing quanta Q_{ion}; the hydrogen density at inner illuminated edge of the nebula $N_H(R_{in})$; the slope γ of the assumed power-law density distribution in H II region: $N_H(R) = N_H(R_{in})\left(\frac{R}{R_{in}}\right)^\gamma$; the filling factor; the relative chemical abundances.

We selected for the comparison with observed data the flux in H_β line, the relative line intesities, the diagnostic ratios between line intensitite as well as ratios between line intensities of the neighbouring ionization stages of the same chemical element, and the size of the ionized region. The criterion of the inconsistency of the modelling results with the observed ones is so-called χ^2-function, that for particular comparison of the modelling value (y^{mod}) and observed one (y^{obs}) of some quantity y with error bars for observed value of $\sigma(y^{obs})$ can be determined as $\chi^2 = \left(\frac{y^{mod}-y^{obs}}{\sigma(y^{obs})}\right)^2$. Thus, optimization task in this form is based on the minimization of the χ^2-function. The using of the independent on the chemical composition diagnostic ratios between line intensities allowed us to divide optimization process into several stages.

At the first stage, the ionization structure of the nebula is determined. During this stage the chemical compositions of the most heavy chemical elements are not varied and have values, obtained from diagnostic methods, and for comparison with observed data are used mainly diagnostic ratios.

At the second stage, the relative chemical abundances are varied at the fixed optimal ionization structure of the nebula obtained from the first stage. At this stage the fluxes in the emission lines are added to the parameters that are used for χ^2-function calculation.

At the third stage, all free parameters and all mentioned above resulting parameters for χ^2-function calculation are used to the finally optimization.

For the calculation of photoionization models we are using G.Ferland's code CLOUDY [29]. This code contains the Peter van Hoof's optizer function *Phymir* (see thesis *http://dissertations.ub.rug.nl/faculties/science/1997/p.a.m.van.hoof/*).

CLOUDY and function *Phymir* were modified for our task realization.

In paper [22,25] it was shown that fluxes in the emission lines of the same ion are not independent. This fact must be taken into account at the freedom degree calculaion. Also, not all selected above free parameters are indepent. In the paper [25] it was shown that some parameters defining ionization structure may be coupled as $P = \frac{U}{(R_{out}^{obs}/R_{in})^{2+\gamma_\epsilon}}$, where $U = \frac{Q_{ion}}{4\pi R_{in}^2 N_H(R_{in})c}$ is the ionization parameters, R_{out}^{obs} corresponds to the observed outer radius of the H II region, and c is the light velocity. Also, varied ionizing fluxes depend on other free parameters defining the nebula ionization structure and on relative abundance He/H [22, 25]. These facts decrease the number of the independent free parameters. Therefore, the freedom degree number must be very careful calculated. The freedom degree number is used to the determination of the error bars for optimal values of free parameters.

It must be noted, that for initialization of the chemical abundances values we use the results of the mentioned above diagnostic method DIAGN [15] upgraded by new ionization correction factors for H II regions and planetary nebulae, and for the ionizing radiation spectrum initialization for H II regions we use our method NLEHII [25] that is independent of any assumption concerning the nature of the ionizing source (see next section). It is very important in the case of the optimal models finding for the small parts of the giant H II region, where observed spectrum was obtained from. In this case we can not use integral ionizing spectrum from all stars in H II regions, that is also very frequently undefined, because we need ionizing radiation fluxes exciting illumination only of the observed nebula part. Thus, without diagnostic methods and methods for the preliminary estimation of the ionizing radiation spectrum, it is impossible to find correctly optimal photoionization model, because too much starting points for optimizer, and too much free parameters even for modern supercomputers.

6 Spectrum of the ionizing radiation

Most nebular objects are ionization bounded. It means that there are embedded into much larger in size cloud of the neutral medium that consist of the neutral gas, molecules, and dust grains. Thus, we can not observe ionizing radiation spectrum ($E_{h\nu} \geq 1Ry$). This spectrum should be determined by theoretical methods. If nebular object surrounds the single star, then ionizing radiation spectrum can be defined from the theoretical stellar athmosphere models. Also, if, in the case of stars cluster, the ionizing source is in the giant H II region, then, if we know the distribution of the stars number over their mass, and also if we know total cluster mass and character of the star formation in this cluster, then total ionizing spectrum from all stars can be obtained. For this purpose STARBURST99 code [35] can be used. But used stellar atmosphere model may be incorrect or very frequently we don't know mentioned above parameters characterizing the ionizing stars cluster, and very rough assumption should be done for ionizing radiation

spectrum determination in above ways.

Therefore, we proposed method (see details in [25, 36] and references therein) for the determination of the energy distribution ionizing spectrum called NLEHII [25]. Ionization-recombination and thermal equilibria are assumed in this method. The continuum at $\lambda \leq 912$Å is divided into three wavelength intervals corresponding to the ionization potentials of H^0, He^0 and He^+ ions: ($'$) $\lambda\lambda 912 - 504$Å, ($''$) $\lambda\lambda 504 - 228$Å, ($'''$) $\lambda\lambda 228 - 22.8$Å. Photons from the first interval are absorbed only by atoms of neutral hydrogen H^0, those from the second interval - by neutral helium He^0 and neutral hydrogen H^0, and those from the third interval - by H^0, He^0 and singly ionized helium He^+. The heavy elements are neglected, because of their much lower abundances. Lyc spectrum in each of these intervals was defined by the flux at the ionization threshould F_{ν_0} and by the spectral index α of the power-law flux dependence on the frequency: $F_\nu = F_{\nu_0} \left(\frac{\nu}{\nu_0}\right)^\alpha$. Thus, Lyc spectrum of the nucleus at the wavelengths shorter $\lambda = 912$Å is defined by 6 parameters (fluxes at the beginning of the each of intervals and the spectral indexes in these intervals). Assuming ionization-recombination equilibrium we obtain 3 equations of photons balance [25, 36, 39]. These equations contain the dependence on the observed fluxes $F(\mathrm{H}\beta)$, $F(\mathrm{He\ I}\ \lambda 4471)$, $F(\mathrm{He\ II}\ \lambda 4686)$ and electron temperature T_e [39].

Additionally, the equation of thermal equlibrium should be added to above three ones. All these equations are described in detail in [25, 36].

A method described by [39] was proposed for the determination of the Lyc spectrum of the planetary nebula nucleus. We have modified this method for the case of the H II region ionized by a stellar cluster. The modification was done by adding to the mentioned above four equations the dependence of the Lyc spectrum shape in ranges $\lambda\lambda 912 - 504$Å and $\lambda\lambda 228 - 22.8$Å on the effective star temperature derived from the stellar atmosphere models from [37, 38] for O-B stars (SdK) [25]. A jump at λ 504Å and shape of a Lyc spectrum in the $\lambda\lambda$ 228-22.8Å wavelength interval can be determined using SdK models most closed to this temperature.

Thus, for the calculation of the Lyc spectrum by this method the observed spectrum of the H II region is required.

We have written a code NLEHII (Nebula Light Excitation: H II regions) in C++ programming language for the fast calculation of the Lyc spectrum.

In each spectrum obtained in such way the procedure for optimization of the number of ionizing photons at $\lambda \leq 228$Å should be used for the observed relative line intensity of the He II $\lambda 4686$ emission line reproducing.

Thus, this method is independent on the assumption about the nature of the ionizing source, and can be used to the separation of nebular photoionization modelling from the tasks on parameters of the stellar atmosphere or parameters of ionizing stars cluster determination. Also, NLEHII can be used to the determination of the ionizing radiation spectrum that excites the illumination of the small part of giant H II region that was observed. We are using this method for the initialization of the ionizing radiation spectrum in optimized photoionization modelling.

7 Superwind bubbles into H II regions and its impact on the ionizing radiation spectrum shape

In our work on optimized photoionization modelling (OPhM) of HII region in blue compact galaxy (BCG) SBS0335-052 [26] it was demonstrated that resulting ionizing radiation spectrum (Lyc-spectra) of the ionizing sources have unclear gap in wavelength range λ 912 – 504Å. Thus, the question become, whether this gap has physical explanation?

All previous photoionization modelling of low-metallicity HII-regions did not take into account the structures created by superwind, which could be present around young starbursts. Such wind forms bubble-like structure which consists of hot cavity irradiating a thermal emission [40,41] with hundred thousand degrees, and thin high density envelope gathered by stellar wind shockwave [40, 42].

For the investigation of the Lyc-spectrum shape transformation during penetrating of the compact stellar wind bubble in paper [44] the three-component photoionization models were culculated. The first component represents low density hot gas, like in stellar wind cavity, that has usually low density and high temperature [40, 42]. In order to conservation of pressure at both sides of contact discontinuity between the first and second components we derived gas density in first component. The second one is a thin envelope of high density gas, compressed by superwind's shockwave. This parameter can be varied in wide range. The third one represents "ordinary"HII region. The size of this component was defined by ionization boundary. Each component represents separate photoionization model, but photoionization in every of these components is caused by both kinds of Lyc-quanta: 1) quanta of direct Lyc-radiation from ionization source (not absorbed in previous component); 2) quanta irradiated into the previous component (diffuse radiation). For the first component, closest to the starburst, the Lyc-spectrum is defined by ionization source.

For the calculations of photoionization models we used, as basis, G.Ferland's code CLOUDY [29] modified for our purposes. For modelling the typical Lyc-spectrum was obtained from OPhM of HII region in blue compact dwarf galaxy SBS 0335-052 [26], excepting above gap presence.

In Fig. 2 the transformation of Lyc-spectrum shape during penetrating by ionizing quanta the first two components is shown. The three curves represent Lyc-spectrum from starburst (solid line), after penetrating hot stellar wind cavity gas (dashed line), and after penetrating of thin dense envelope (second component) correspondingly. It can be seen from Fig. 2, as we expected, the gap in spectrum within wavelength λ 912 – 504Å is present in Lyc-spectra after penetrating thin dense envelope. It is because photons energy dependence of cross section, σ_ν, for hydrogen like ions has a peak at it's ionization potential, and then rapidly decreases with increasing of photons energy [5]. Since photon's free path in environment with density n is defined as $l_\nu = 1/(\sigma_\nu n)$, in the case of high density envelope, photons with energy close to the ionization potential will be absorbed, while the other ones, with higher energy, will cross the envelope.

Thus, the parameters of the ionizing stars cluster can be determined from the fit of Lyc-spectrum obtained by STARBURST99 to the one obtained using optimized photoionization modelling, but previously Lyc-spectrum transformation by the possibly presented slellar superwind cavity should be taken into account.

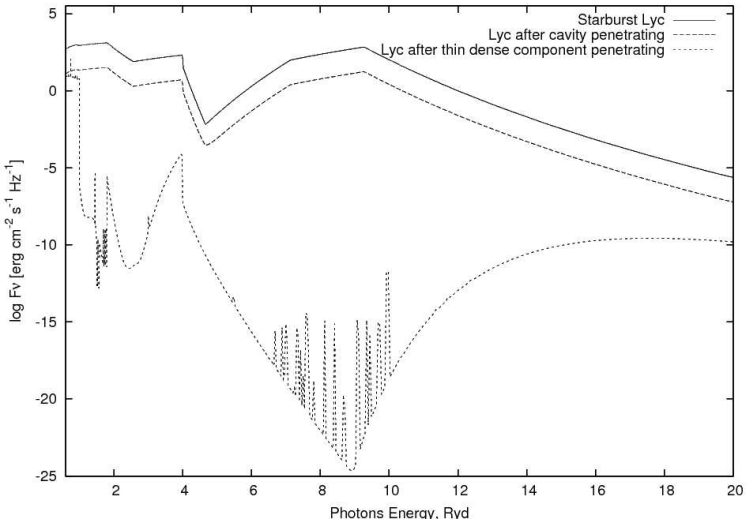

Рис. 2: Lyc-spectrum transformation: HII region with stellar superwind bubble inside.

At present we are caclulating large grid of the multicomponent photoionization models for different age of the the central starburst. The aim is to estimate dependences between starburst parameters and efficiency of the Lyc-spectrum transformation as well as we are looking for ratios between line intensities sensitive to the stellar superwind cavity presence inside H II region.

We also plan to implement stellar wind cavity model into optimized photoionization modelling.

At present we see that understanding of the physical processes into nebular objects is impossible without precise photoionization modelling.

The bibliography

1. *Hoskin M.* Unfinished Business: William Herschel's Sweeps for Nebulae / Hoskin M. // History of Science. – 2005. – Vol.43. P.305-320.
2. *Kenneth G.J.* Messierś nebulae and star clusters / Kenneth G.J. – Cambridge: Cambridge University Press, 1991. – 435 p.
3. *Bowen I.S.* The origin of the nebular lines and the structure of the planetary nebulae / Bowen I.S. // Astrophysical Journal. – 1928. – Vol. 67. P.1-15.
4. *O'Dell C.R.* The Orion Nebula and its associated population / O'Dell C.R. // Annual Review Astronomy and Astrophysics. – 2001. – Vol. 39(1). – P.99-136.
5. *Osterbrock D. E.* Astrophysics of Gaseous Nebulae and Active Galactic Nuclei. Second Edition/ Osterbrock D. E. & Ferland G. J. – Saulito, California: University Science Book, ISBN 1-891389-34-3, 2005. – 461 p.
6. *Garnet D.R.* Electron temperature variations and the measurement of nebular abundances/ Garnet D.R. // Astron. J.. – 1992. – Vol. 103, No. 4. – P. 1330-1337.

7. *Pagel B.E.J.* The primordial helium abundance from observation of extragalactic H II regions / Pagel B.E.J., Simonson E.A., Terlevich R.J. & Edmunds M. G. // Monthly Notices Roy. Astron. Soc. – 1992. – Vol. 255, No. 2. – P.325-345.
8. *Pagel B.E.J.* On the Composition of H II regions in southern galaxies. Soc. // Pagel B.E.J., Edmunds M.G., Blackwell D.E., Chun M.S. & Smith G. // Monthly Notices Roy. Astron. Soc. – 1979. – Vol. 189, No. 1. – P.95-113.
9. *Dopita M.A.* Theoretical models for H II regions. The extragalactic H II region abudance sequence / Dopita M.A. & Evans I.N. // Astrophys. J. – 1986. – Vol. 307, No.1. – P.431-440.
10. *Edmunds M.G.* On the composition of H II regions in southern galaxies - III. NGC 2997 and 7793 / Edmunds M.G. & Pagel B.E.J. // Monthly Notices Roy. Astron. Soc. – 1984. – Vol. 211. – P.507-519.
11. *McCall M.L.* The chemistry of galaxies. I. The nature of giant extragalactic H II regions / McCall M.L., Rybski P.M. & Shields G.A. // Astrophys. J. Suppl. Ser. – 1985. – Vol. 57, No.1. – P.1-62.
12. *Zaritsky D.* H II regions and the abundance properties of spiral galaxies / Zaritsky D., Kennicutt R.C. & Huchra J.P. // Astrophys. J. – 1994. – Vol. 420, No.1, P.87-109.
13. *Pilygin L.S.* On the oxygen abundance determination in H II regions. The problem of the line intetensities-oxigen abundance calibration / Pilygin L.S. // Astronomy and Astrophysics – 2000. – Vol. 362, No. 2. – P.325-332.
14. *Pilyugin L.S.* (2001). On the oxygen abundance determination in H II region. Highmetallicity regions / Pilyugin L.S.// Astron. and Astrophys. – 2001. – Vol. 369, No. 2. – P.594-604.
15. *Holovatyy V.V.* Quantitative Analysis of the Ultraviolet, Optical and Infrared emission spectra of the celestial bodies with the determination aim of the physical parameters and the chemical composition of the irradiating diffuse material, and the interstellar absorption (Rus.) / Holovatyy V.V., Gershberg R.E., Mal'kov Yu.F. & Pronik, V.I. // Izvestia Krymsk. Astroph. Obs. – 1999. – Vol. 96. – P.72-138.
16. *Shaw R.A.* Software for the Analysis of Emission Line Nebulae / Shaw R.A., & Dufour R.J. // Publications of the Astronomical Society of the Pacific. – 1995. – Vol. 107. – P.896-906.
17. *Stasinska G.* A grid of model HII regions for extragalactic studies / Stasinska G. // Astronomy and Astrophysics Suppl. Ser. – 1990. – Vol.83. – P.501-538.
18. *Holovatyi V.V.* Ionization correction factors for H II regions in blue compact dwarf galaxies / Holovatyi V.V. & Melekh B.Ya. // Kinematika i Fizika Nebesnykh Tel. – 2002. – Vol. 18, No.4. – P.362-375.
19. *Holovatyi V.V.* The Chemical Composition of HII Regions in Blue Compact Dwarf Galaxies / Holovatyi V.V. & Melekh B.Ya // Astronomy Reports. – 2002. – Vol. 46, Issue 10. – P.779-790.
20. *Havrylova N.V.* (2002). Ionization-Correction Factors for the Chemical Composition Determination of Planetary Nebulae with Inhomogeneity Nebular Gas Distribution / Havrylova N.V., Holovatyy V.V. & Melekh B.Ya // Journal of Physical Studies. – 2002. – Vol. 6, Issue 4. – P.451-454.
21. *Holovatyi V.V.* (2003). Chemical Composition of Galactical Planetary Nebulae / Holovatyi V.V. & Havrylova N.V. // Journal of Physical Studies. – 2003. – Vol. 7,Issue 4. – P.461-467.

22. *Holovatyi V.V.* The Chemical Composition of HII Regions in Blue Compact Dwarf Galaxies / Holovatyi V.V. & Melekh B.Ya. // Astronomy Reports. – 2005. – Vol. 49, Issue 8. – P.595-603.
23. *Melekh, B.Ya.* Optimized Photoionization Modelling of H II Region in Blue Compact Dwarf Galaxy SBS 0940+544 / Melekh, B.Ya. // Journal of Physical Studies. – 2006. – Vol. 10, Issue 2. – P.148-159.
24. *Havrylova N.V.* Optimized photoionization models of the planetary nebula NGC 6720 / Havrylova N.V., Holovatyy V.V. & Melekh B.Ya. // Astrophysics and Cosmology After Gamow, ed. by G. S. Bisnovaty-Kogan, S. Silich, E. Terlevich, R. Terlevich and A. Zhuk. – Cambridge, UK: Published by Cambridge Scientific Publishers, ISBN: 978-1-904868-5, 2007. – P.407.
25. *Melekh B.Ya.* Determination of the physical parameters, Lyman continua, and chemical compositions of HII regions in blue compact dwarf galaxies / Melekh B.Ya., Holovatyi V.V. & Izotov Yu.I. // Astronomy Reports. – 2008. – Vol. 52, Issue 3. – P.184-200.
26. *Melekh B.Ya.* Two-Stages Optimized Photoionization Modelling of HII Region in Blue Compact Galaxy SBS 0335-052 / Melekh B.Ya. // Journal of Physical Studies. – 2009. – Vol. 13, No.3. – P.3901-1-3901-16.
27. *Henney W.J.* (2007). How to Move Ionized Gas: An Introduction to the Dynamics of HII Regions / Henney W.J. // Diffuse Matter from Star Forming Regions to Active Galaxies - A Volume Honouring John Dyson, Edited by T.W. Hartquist, J. M. Pittard, and S. A. E. G. Falle. Series: Astrophysics and Space Science Proceedings, P.103-129 ISBN-10 1-4020-5424-6 (HB); ISBN-13 978-1-4020-5424-2 (HB); ISBN-10 1-4020-5425-4 (e-book); ISBN-13 978-1-4020-5425-9 (e-book); Springer Dordrecht, 2007. – p.103
28. *Henney W.J.* (2005) Self-Consistent Dynamic Models of Steady Ionization Fronts. I. Weak-D and Weak-R Fronts / Henney W.J., Arthur S.J., Williams R.J.R. & Ferland G.J. // The Astrophysical Journal. – 2005. – Vol. 621, Issue 1. – P.328-347.
29. *Ferland G.J.* (2005) Hazy, a Brief Introduction to Cloudy/ Ferland G.J. – University of Kentucky, Department of Physics and Astronomy: Internal Report, 2005. – 863 p.; *www.nublado.org*
30. *Morisset C.* Modelling of Asymmetric Nebulae. II. Line Profiles / Morisset C., Stasinska G. // Revista Mexicana de Astronomia y Astrofisica. – 2006. – Vol. 42. – P.153-166.
31. *Gruenwald R.* A New Generation of Photoionization Codes: Three-dimensional Models. The Bipolar Planetary Nebula IC 4406 / Gruenwald R., Viegas S.M. & Broguiere D. // Astrophysical Journal. – 1997. – Vol. 480. – P.283-289.
32. *Ercolano B.* X-Ray Enabled MOCASSIN: A Three-dimensional Code for Photoionized Media / Ercolano B., Young P.R., Drake J.J. & Raymond J.C. // The Astrophysical Journal Supplement Series. – 2008. – Vol. 175, Issue 2. – P.534-542.
33. *Dumont A.-M.* Escape probability methods versus “exact"transfer for modelling the X-ray spectrum of Active Galactic Nuclei and X-ray binaries / Dumont A.-M., Collin S., Paletou F., CoupГ© S., Godet O. & Pelat D. // Astronomy and Astrophysics. – 2003. – Vol. 407. – P.13-30.
34. *Olson G.L.* A rapidly convergent iterative solution of the non-LTE line radiation transfer problem / Olson G.L., Auer L.H. & Buchler J.R. // J. Quant. Spectrosc.

Radiat. Transfer. – 1986. – Vol. 35. – P.431-442.
35. *Leitherer C.* Starburst99: Synthesis Models for Galaxies with Active Star Formation / Leitherer C., Schaerer D., Goldader J.D., Delgado R.G., Robert C., Kune D.F., de Mello D.F., Devost D. & Heckman T.M. // Astrophysical Journal Supplement Series. – 1999. – Vol. 123. – P.3-40.
36. *Melekh B.Ya.* (2000). Energy distribution in the emission spectra of HII region nucleus in the blue compact dwarf galaxies beyond λ 912Å/ Melekh B.Ya. // Journal of Physical Studies. – 2000. – Vol. 4, Issue 2. – P.225-235.
37. *Schaerer D.* Combined stellar structure and atmosphere models for massive stars. I. Interior evolution and wind properties on the main sequence / Schaerer D., de Koter A., Schmutz W. & Maeder A. // Astronomy and Astrophysics. – 1996. – Vol.310. – P.837-848.
38. *Schaerer D.* Combined stellar structure and atmosphere models for massive stars. II. Spectral evolution on the main sequence / Schaerer D., de Koter A., Schmutz W. & Maeder A. // Astronomy and Astrophysics. – 1996. – Vol.312. – P.475-495.
39. *Golovaty V.V.* The Energy Distribution in Lyman Continuum and the Effective Temperatures of Planetary Nebulae Nuclei / Golovaty V.V. & Pronik V.I. // ASTROFIZIKA. – 1990. – Vol. 32, No.1. – P.99-116.
40. *Bochkarev N.G.* X-Ray Emission from Certain Nebulae Formed by Stellar Wind / Bochkarev N.G. & Zhekov S.A. // Sov. Astron. – 1990. .– Vol. 34. – P.138-146.
41. *Raymond J.C.* Soft X-ray spectrum of a hot plasma / Raymond J.C. & Smith B.W. // Astroph. J. Suppl. Ser. – 1977. – Vol. 35. – P.419-439.
42. *Weaver R.* Interstellar bubbles. II - Structure and evolution / Weaver R., McCray R., Castor J., Shapiro P. & Moore R. // Astroph. J. – 1977. – Vol. 218. – P.377-395.
43. *Rodriguez-Franco A.* A High-Density Thin Layer Confining the H II Region M42: Heinrich Hertz Telescope Measurements / Rodriguez-Franco A., Wilson T.L., Martin-Pintado J. & Fuente A. // // Astroph. J. – 2001. – Vol.559. – P.985-992.
44. *Kozel R.V.* Photoionization Modelling of HII Region with Stellar Wind Bubble Inside / Kozel R.V. & Melekh B.Ya. // YSC'16 Proceedings of Contributed Papers, (eds. Choliy V. Ya., Ivashchenko G. – 2009. – P.37-41.

Стаття надійшла до редакції 9.5.2012
прийнята до друку 17.10.2012

ОГЛЯД НЕБУЛЯРНОЇ АСТРОФІЗИКИ

Б. Мелех

Львівський національний університет імені Івана Франка, вул. Кирила і Мефодія, 8, 79005 Львів, Україна

Подано короткий огляд історії досліджень небулярних об'єктів. Описано основні сучасні методи визначення фізичних характеристик та хімічного вмісту у різноманітних небулярних середовищах. Розглянуто нові підходи до досліджень планетарних туманностей та зон HII, розроблені на кафедрі астрофізики Львівського національного університету, а також нові фізичні результати, які вдалось отримати завдяки цим підходам.

Ключові слова: планетарні туманості, HII регіони, фотоіонізаційне моделювання, діагностика емісійних ліній.

ОБЗОР НЕБУЛЯРНОЙ АСТРОФИЗИКИ

Б. Мелех

Львовский национальный университет имени Ивана Франко, ул. Кирилла и Мефодия 8, 79005 Львов, Украина

Дан краткий обзор истории исследования небулярных объектов. Описаны основные методы определения физических характеристик и химического состава различных небулярных сред. Рассматриваются новые подходы к исследованию планетарных туманностей и HII регионов, разработанные на кафедре астрофизики Львовского национального университета, а также новые физические результаты, полученные благодаря этим походам.

Ключевые слова: планетарные туманости, HII регионы, фотоионизационное моделирование, диагностика емисионных линий.